





Characterizing nuclear modification effects in high-energy O-O collisions at energies available at the CERN Large Hadron Collider: A transport model perspective

Debadatta Behera ^{1,*}, Suman Deb ^{2,†}, Captain R. Singh ^{1,‡} and Raghunath Sahoo ^{1,§}

¹Department of Physics, Indian Institute of Technology Indore, Simrol, Indore 453552, India

²Laboratoire de Physique des 2 infinis Irène Joliot-Curie, Université Paris-Saclay, CNRS-IN2P3, F-91405 Orsay, France



(Received 14 August 2023; revised 28 October 2023; accepted 21 November 2023; published 11 January 2024)

The present work focuses on oxygen-oxygen (O-O) collisions, which are planned at the CERN Large Hadron Collider. Oxygen, being a doubly magic number nucleus, has some very unique features. This study attempts to probe the exotic state of QCD matter in O-O collisions. Additionally, the role of different nuclear density profiles in governing the final-state dynamics in ultrarelativistic nuclear collisions is also explored. Using a multiphase transport model, we obtain the nuclear modification factor (R_{AA}) for all charged hadrons and identified particles for O-O collisions at $\sqrt{s_{NN}} = 7$ TeV. Furthermore, we investigate the behavior of R_{AA} as a function of transverse momentum (p_T) for three centralities (most central, mid-central, and peripheral) considering both α -cluster and Woods-Saxon nuclear density profiles. We also extend this work to study the rapidity dependence of R_{AA} for all charged hadrons. To better understand our findings of O-O collisions, the results are confronted with the available data of R_{AA} for Pb-Pb collisions. The present study sheds light on particle production mechanisms, emphasizing factors influencing particle yield from precollision to postcollision stages in the context of O-O collisions.

DOI: [10.1103/PhysRevC.109.014902](https://doi.org/10.1103/PhysRevC.109.014902)

I. INTRODUCTION

Ultrarelativistic hadronic and nuclear collisions at the Large Hadron Collider (LHC) have elevated physics to an entirely new level. Heavy-ion collisions at the LHC have facilitated the exploration of hot and dense QCD matter known as quark-gluon plasma (QGP). Hints of the existence of QCD matter, beyond heavy-ion collisions, have also been observed in the high multiplicity of p -Pb and pp collisions at LHC energies [1,2]. In this context, the future run at the LHC is expected to include a short run of O-O collisions [3]. This brief run involving oxygen nuclei could provide a valuable opportunity to investigate the observed effects in high-multiplicity p -Pb collisions, with a system having a relatively larger geometrical transverse overlap area but with a similar small number of participating nucleons and a similar number of final-state multiplicity [4]. It is expected that a larger overlap area combined with approximately similar final-state multiplicity would enhance path-length-dependent effects such as jet quenching. Recently, several theoretical investigations

such as those in Refs. [5–11], explored various aspects of particle production dynamics related to O-O collisions. In addition, O-O collisions provide an excellent opportunity to study the underlying mechanisms responsible for transverse collective flow effects, particle production, and light-nuclei production in a multiplicity range that bridges pp and p -Pb on the lower side, and Xe-Xe and Pb-Pb on the higher side [4].

Apart from these, the ^{16}O has a reasonably compact structure and is resilient against decay due to its double magic property [12]. Furthermore, it is hypothesized that the α -clustered structure [13,14] has an additional impact on the oxygen nuclei. A comprehensive analysis of the α -clustered oxygen nucleus is presented in Ref. [13]. Therefore, it is also important to investigate whether the initial nuclear structure affects the final-state observables, such as net particle production yield, the collective behavior of produced particles, etc. Thus, it is crucial to comprehend these observables as well as QGP-like properties while studying systems produced in O-O collisions.

Several studies have focused on understanding the characteristics of the quark-gluon plasma (QGP) in collisions of varying sizes, energies, and hence final-state multiplicities. It has been shown in Ref. [8] that Pb-Pb collisions have a 60% larger radius in comparison to O-O collisions at the same multiplicity. However, central O-O collisions exhibit significantly smaller eccentricities and higher temperatures than Pb-Pb collisions with the same multiplicity [3]. Another interesting finding is that as the system size decreases, there is a more direct relationship between the initial eccentricity and the flow harmonics. To better understand QGP-like effects, it is crucial to study observable behavior in different collision

*debadatta3337@gmail.com

†sumandeb0101@gmail.com

‡captainriturajsingh@gmail.com

§Corresponding author: Raghunath.Sahoo@cern.ch

Published by the American Physical Society under the terms of the [Creative Commons Attribution 4.0 International](https://creativecommons.org/licenses/by/4.0/) license. Further distribution of this work must maintain attribution to the author(s) and the published article's title, journal citation, and DOI. Funded by SCOAP³.

systems with the same multiplicity at the LHC. This approach would greatly benefit experimental efforts. One possible way to investigate this idea is to compare observables sensitive to medium properties across different system sizes. In a nutshell, the investigation of the ultrarelativistic O-O collisions at the LHC energy would play a crucial role in the field of high-energy physics with the new notion of final-state multiplicity driving the system properties while bridging the gap across relevant colliding species and centralities.

In Sec. I, we emphasized why O-O collisions are crucial. Further, the paper is organized into four sections. In Sec. II, we delve into the event generation methodology and briefly present the formalism employed. The obtained results are thoroughly examined and discussed in Sec. III. Finally, we conclude the paper by summarizing the main findings in Sec. IV and providing a potential outlook for future research.

II. EVENT GENERATION AND ANALYSIS METHODOLOGY

In this section, we give a brief overview of the AMPT model and discuss the Woods-Saxon and α -clustered nuclear structure of the oxygen nucleus. At the end of this section, we have defined the nuclear modification factor, R_{AA} .

A. A multiphase transport (AMPT) model

A multiphase transport model (AMPT) is a simulation framework for studying high-energy heavy-ion collisions. It consists of four main stages: initialization, parton cascade, hadronization, and hadron rescatterings [15,16]. In the initialization stage, the initial conditions for the collisions are generated using the HIJING model [17]. This includes information about the spatial and momentum distributions of minijet partons and soft string excitations. The parton cascade stage is carried out using Zhang's parton cascade (ZPC) model [18]. This stage simulates the interactions between partons and controls the partonic cross section based on the values of the strong coupling constant (α_s) and the Debye screening mass (μ). Once the partons freeze out, the AMPT model uses a coalescence mechanism to combine them into hadrons; this process is called hadronization. After hadronization, the dynamics of the subsequent hadronic rescatterings are described by a relativistic transport (ART) model. This stage accounts for the interactions and collisions among the produced hadrons. In this particular study, we use the string melting mode of the AMPT model (version 2.26t9b) with Lund fragmentation parameters $a = 0.3$, $b = 0.15 \text{ GeV}^{-2}$, and parton cross section $\sigma_{gg} = 3 \text{ mb}$ for both oxygen-oxygen (O-O) [5,13] and lead-lead (Pb-Pb) collisions. Lund fragmentation parameters for proton-proton (pp) collisions use $a = 0.5$ and $b = 0.9 \text{ GeV}^{-2}$ with $\sigma_{gg} = 3 \text{ mb}$ [19]. Experimental data from pp collisions [20–23] are utilized to compare the transverse momentum spectra [20–23].

In the context of heavy-ion collisions, the Woods-Saxon distribution is commonly used to represent the density profile of a nucleus. The Woods-Saxon charge density, based on a

3pF (three-parameter Fermi) distribution, is defined as;

$$\rho(r) = \frac{\rho_0 \left[1 + w \left(\frac{r}{r_0} \right)^2 \right]}{1 + \exp\left(\frac{r-r_0}{a}\right)}. \quad (1)$$

Here, r_0 is described as an equilibrium or saturation radius up to which nuclear matter is evenly distributed, and corresponding density distribution is defined by ρ_0 (a constant nuclear density at the core of a nucleus). While r is the radial distance, w is the deformation parameter, and a is the skin depth of the nucleus. For the oxygen nucleus, $r_0 = 2.608 \text{ fm}$, $a = 0.513 \text{ fm}$, and $w = -0.051$ according to Refs. [14,24–27].

Recent theoretical studies have indicated the presence of α -clustered structure in the ^{16}O - ^{16}O nucleus [14,24–27]. In our study, we incorporated the α -clustered structure into the oxygen nucleus using the AMPT model. This implementation was done numerically, where four ^4He nuclei were positioned at the vertices of a regular tetrahedron structure. Each ^4He nucleus follows the Woods-Saxon density profile described by Eq. (1), with the parameters $r_0 = 0.964 \text{ fm}$, $a = 0.322 \text{ fm}$, and $w = 0.517$. The root-mean-square (rms) radius of ^4He is determined to be 1.676 fm . The α -clustered nuclei are arranged at the vertices of the tetrahedron, which has a side length of 3.42 fm . The root-mean-square (rms) radius of the oxygen nucleus is calculated to be 2.6999 fm . More details about the α -clustered implementation in the AMPT model can be found in Refs. [13,28].

B. R_{AA} : Applicability and comparison

In this work, we investigate the nuclear modification factor (R_{AA}) for all-charged hadrons and identified particles in O-O collisions at $\sqrt{s_{NN}} = 7 \text{ TeV}$. Table I presents number of binary collisions ($\langle N_{\text{coll}} \rangle$) determined from Glauber model, number of participating nucleons ($\langle N_{\text{part}} \rangle$) obtained from both Glauber and AMPT model, and the average charged-particle multiplicity ($\langle dN_{ch}/d\eta \rangle$) from AMPT and ALICE [29] for O-O [13] and Pb-Pb collisions at $\sqrt{s_{NN}} = 7 \text{ TeV}$ and 5.02 TeV , respectively, at midrapidity. The results displayed in Table I indicate that the $\langle dN_{ch}/d\eta \rangle$ for the α -clustered density profile for (0–5)% of O-O collisions are approximately equivalent to the ALICE [29] Pb-Pb collisions for (50–60)% centrality. This is a striking observation concerning the role of multiplicities in relation to thermalization in small systems, as studied by Landau in 1953 [30], and extended later in 1982 by van Hove, who explored the possibility of a quark-hadron phase transition in small systems using multiplicity as a probe [31]. This highlights the importance of multiplicities in the exploration of understanding the consequence of produced QCD medium. Additionally, in our previous work [13], we observed that the initial energy density produced in all collision centralities in O-O collisions are higher than the lattice QCD-predicted threshold for a deconfinement transition. This suggests the potential to create a QGP-like state even in oxygen nucleus collisions. Therefore, it is of interest to examine how the medium formed in two different colliding systems (O-O and Pb-Pb), which have different geometric overlap sizes [8] but approximately similar numbers of final-state charged-particle

TABLE I. Average charged particle multiplicity density ($\langle dN_{ch}/d\eta \rangle$) [ALICE [29] and AMPT], number of participating nucleons ($\langle N_{part} \rangle$) (AMPT and Glauber) and number of binary collisions ($\langle N_{coll} \rangle$) (Glauber) for O-O collisions [13] at $\sqrt{s_{NN}} = 7$ TeV and Pb-Pb system $\sqrt{s_{NN}} = 5.02$ TeV in the range $|\eta| < 0.5$.

System	$\sqrt{s_{NN}}$ (TeV)	Centrality (%)	$\langle N_{part} \rangle$ (Glauber)	$\langle N_{part} \rangle$ (AMPT)	$\langle N_{coll} \rangle$ (Glauber)	$\langle dN_{ch}/d\eta \rangle$
O-O, α -cluster	7	0–5	29.43 ± 2.02	30.73 ± 2.06	55.12 ± 8.90	187.54 ± 0.14
O-O, Woods-Saxon	7	0–5	28.00 ± 2.06	29.26 ± 1.99	48.33 ± 9.43	161.07 ± 0.15
Pb-Pb	5.02	50–60	53.6 ± 1.2	50.20 ± 7.04	90.88 ± 33.00	183.00 ± 8.00 [ALICE] 235.25 ± 0.56 [AMPT]

multiplicity at specific centralities, affects particle production dynamics. However, an expected comparable $\langle dN_{ch}/d\eta \rangle$ for Pb-Pb collisions obtained from AMPT simulation and the estimation of ALICE experimental results show a discrepancy, as seen in Table I. This discrepancy could be attributed to the AMPT model's inadequacy to explain some experimental results, as discussed in Refs. [19,32]. Consequently, we proceed with studying the behaviors of R_{AA} obtained from AMPT simulation of O-O collisions at (0–5)% centrality and ALICE results of (50–60)% centrality in Pb-Pb collisions, as multiplicities in these centralities are comparable. To provide a comprehensive and comparative conclusion, we consider both Woods-Saxon and α -clustered nuclear density profiles for oxygen nuclei.

The well-known form of R_{AA} is given as;

$$R_{AA} = \frac{d^2N^{AA}/dp_T d\eta}{\langle N_{coll} \rangle d^2N^{pp}/dp_T d\eta}, \quad (2)$$

where N_{AA} and N^{pp} are the charged-particle yields in A - A and pp collisions, respectively. The mean number of binary collisions is $\langle N_{coll} \rangle = \sigma_{inel}^{NN} \langle T_{AA} \rangle$, where σ_{inel}^{NN} is the total inelastic nucleon-nucleon cross section and $\langle T_{AA} \rangle$ is the mean nuclear thickness function. The $\langle N_{coll} \rangle$ values for O-O collisions are taken from Ref. [13], and for the Pb-Pb collisions, it is obtained via the impact parameter determination in the Glauber model [33–35].

III. RESULTS AND DISCUSSIONS

In this section, we first focus on evaluating the accuracy of the AMPT simulated data by comparing the transverse momentum (p_T) spectra in pp and Pb-Pb collisions with the corresponding ALICE experimental results. Next, we obtained the nuclear modification factor for charged hadrons in O-O collisions at $\sqrt{s_{NN}} = 7$ TeV. To examine the effect of scaling on the estimation of the nuclear modification factor in the work, we have used both ALICE experimental and AMPT simulated data for the respective yields from pp collisions. We define R_{AA}^{Exp} (R_{AA}^{AMPT}) for the case where scaling is done using ALICE experimental (AMPT simulated) data. However, corresponding yields from O-O and Pb-Pb collisions are taken from the AMPT simulation only. The influence of the Woods-Saxon and α -clustered nuclear structures on the nuclear modification factor, taking into account identified particles, is also estimated. This observable, having dependence on fundamental quantities such as rapidity (y), is very likely to be sensitive to the choice of the phase space. In order to take this fact into account, we have also investigated the

dependence of the nuclear modification factor on the rapidity (y) and centrality of the collisions.

A. Validation of the simulation via p_T spectra

The particle production yield and/or particle transverse momentum (p_T) spectra play a crucial role in exploring the particle production mechanisms in ultrarelativistic collisions. The study of high- p_T particle production and parton energy loss provide insights into the dynamics of QCD matter. The partons experience energy loss as they traverse through a medium, which causes the parton splitting and gluon emission. Understanding the mechanism of parton energy loss is thus one of the primary goals of heavy-ion collisions. The energy loss can be determined by comparing the p_T spectra of pp collisions with heavy-ion collisions at the same energy. Understanding the precise method by which hard particles lose energy while traversing through the medium requires a thorough investigation of R_{AA} . However, estimation of this observable requires input from both pp and heavy-ion collisions as shown in Eq. (2) and thus, first of all, p_T spectra of all charged particles obtained from AMPT are compared with ALICE results, to validate the simulation tuning. Figure 1 shows this comparison in Pb-Pb collisions at $\sqrt{s_{NN}} = 5.02$ TeV for (50–60)% centrality, and Figs. 2 and 3 shows the comparison of charged particles p_T spectra in pp collisions at $\sqrt{s} = 5.02$ TeV (7 TeV) for minimum bias. This comparison reveals that the spectral shape from AMPT agrees well with the experimental data towards high- p_T (>4 GeV), while there is a reasonable degree of deviation from the experimental results towards low- p_T range. However, within uncertainties, this also validates that the tuning of the AMPT simulation used in this work quantitatively matches the experimental results within the acceptance range. Figures 4 and 5 shows the comparison of p_T spectra of identified particles obtained from both the ALICE experimental [22,23] and AMPT simulated data at $\sqrt{s} = 5.02$ (7) TeV. These comparisons reveal that, when accounting for uncertainties, pions from AMPT exhibit relatively good agreement with the experimental data, particularly in the high- p_T region. However, both kaons and protons exhibit significant deviations. As we shift towards low- p_T ranges (<1 GeV), it becomes evident that kaons and protons align more closely with the experimental data, while a noticeable discrepancy remains in the case of pions. It is worth mentioning here that the scaling of R_{AA} in the rest of the paper is done considering p_T spectra in pp collisions from both ALICE [20–23] and AMPT.

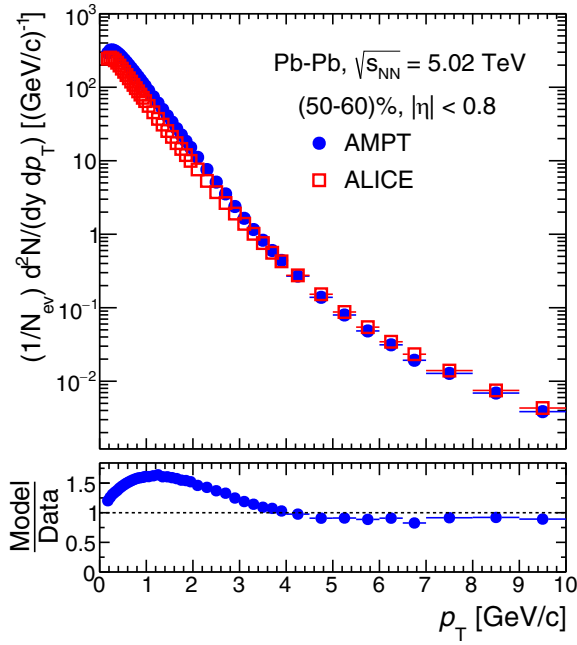


FIG. 1. Comparison of charged particles p_T spectra obtained from AMPT for Pb-Pb collisions at $\sqrt{s_{NN}} = 5.02$ TeV with ALICE results [21]. Statistical errors are within the markers.

With the above comparison and validation of the simulation, we proceed to obtain R_{AA} in ultrarelativistic O-O collisions. This system lies between Pb-Pb and pp collisions species with respect to the final-state multiplicity [36]. Though, in the MC-Glauber model calculation, it is reported

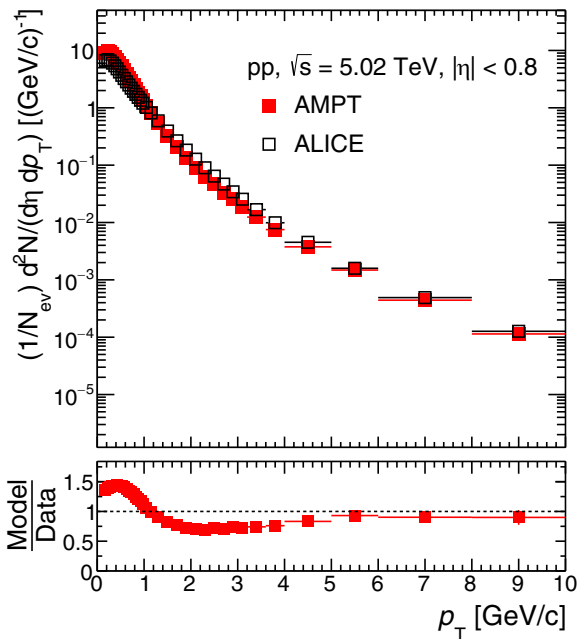


FIG. 2. Comparison of charged particles p_T spectra obtained from AMPT for pp collisions at $\sqrt{s} = 5.02$ TeV with ALICE results [21]. Statistical errors are within the markers.

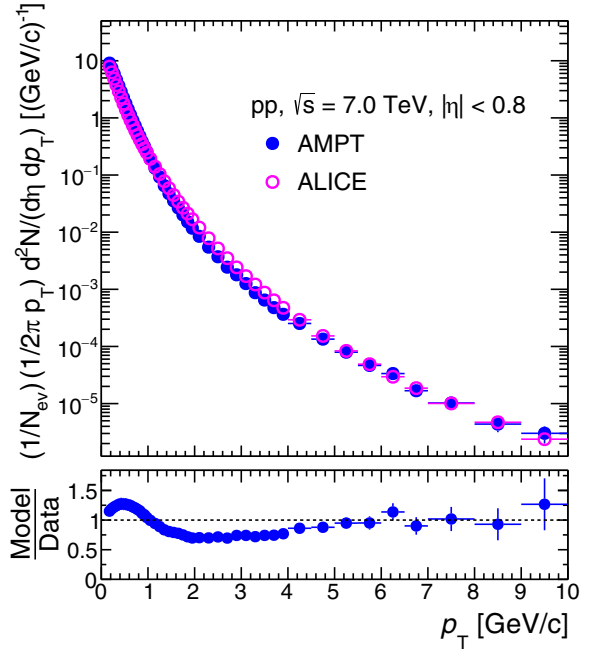


FIG. 3. Comparison of charged particles p_T spectra obtained from AMPT for pp collisions at $\sqrt{s} = 7$ TeV with ALICE results [20]. Statistical errors are within the markers.

that the mean number of participants ($\langle N_{part} \rangle$) in most central (0–5)% O-O collisions are comparable with the $\langle N_{part} \rangle$ in peripheral (60–70)% Pb-Pb collisions [13,37]. However, it has also been observed that the charged-particle multiplicity obtained from AMPT simulation of O-O collisions

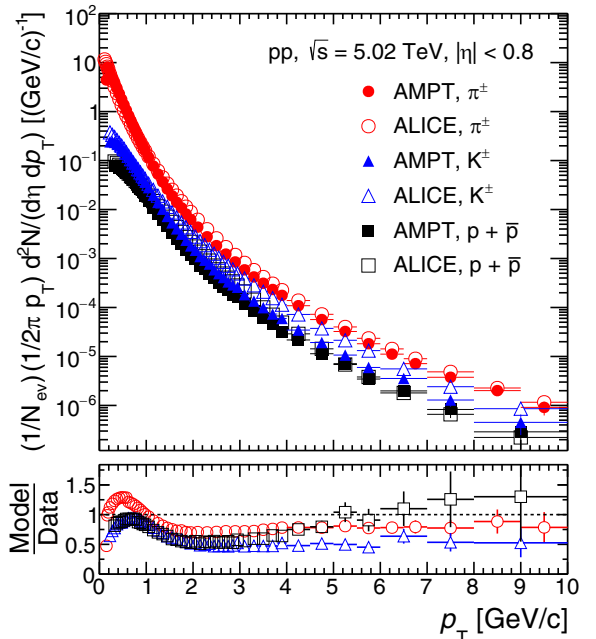


FIG. 4. Comparison of identified particles p_T spectra obtained from AMPT for pp collisions at $\sqrt{s} = 5.02$ TeV with ALICE results [22]. Statistical errors are within the markers.

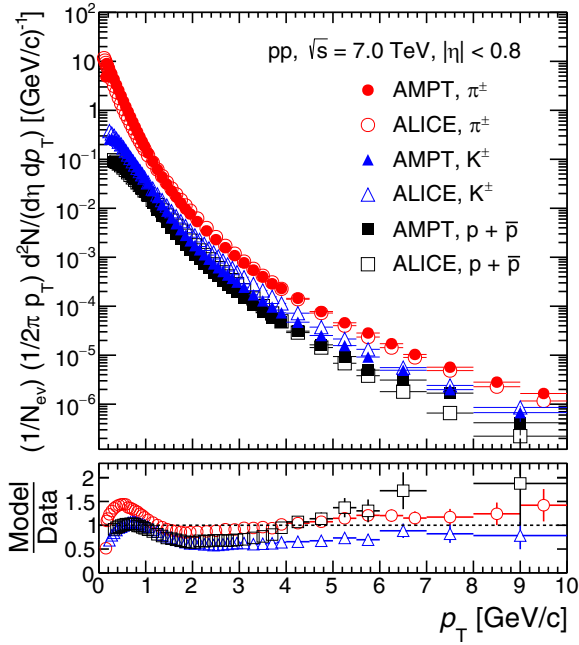


FIG. 5. Comparison of identified particles p_T spectra obtained from AMPT for pp collisions at $\sqrt{s} = 7$ TeV with ALICE results [23]. Statistical errors are within the markers.

corresponding to the (0–5)% centrality class approximately agrees with the (50–60)% centrality of the Pb-Pb collisions [13]. Thus, this fact is expected to show up in the p_T spectra as well. In Fig. 6, we have obtained charged-particle p_T

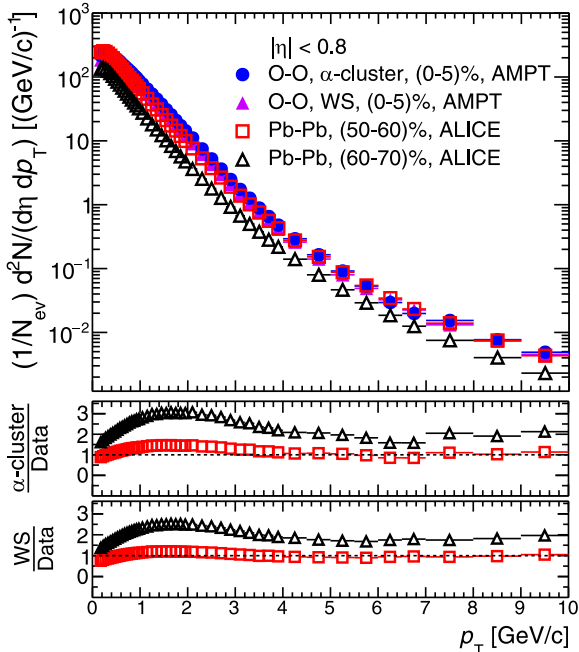


FIG. 6. Comparison of charged particles p_T spectra of (0–5)% from AMPT result for O-O at $\sqrt{s_{NN}} = 7$ TeV with (50–60)% and (60–70)% of ALICE results [21] for Pb-Pb collisions at $\sqrt{s_{NN}} = 5.02$ TeV. Statistical errors are within the markers.

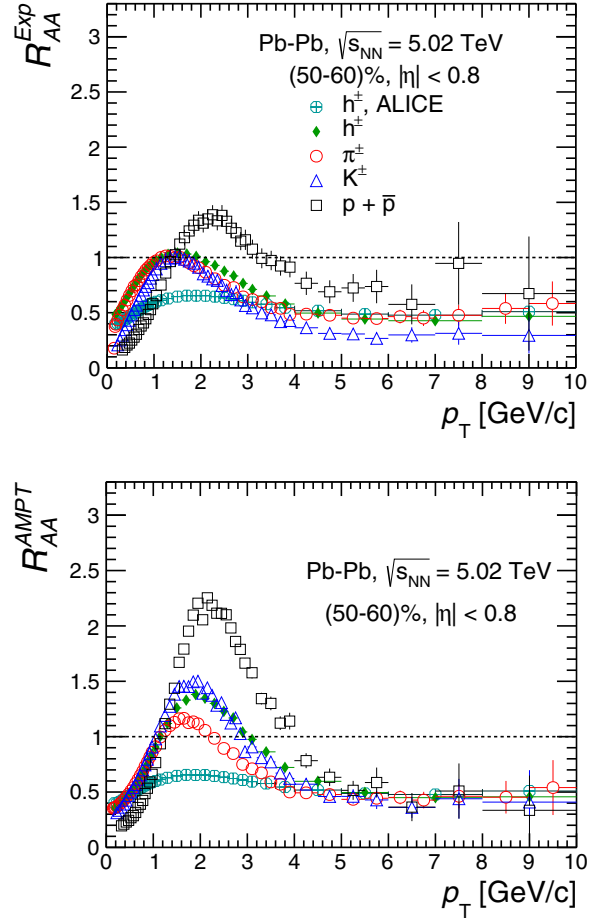


FIG. 7. Nuclear modification factor of charged hadrons and identified particles in Pb-Pb collisions at $\sqrt{s_{NN}} = 5.02$ TeV for (50–60)%, considering the pp yield from experimental data (ALICE) and Pb-Pb yield from AMPT simulation (top). In the bottom panel, we show the nuclear modification considering both the pp and Pb-Pb yields from AMPT simulation [21].

spectra for the most central O-O collisions considering both α -clustered and Woods-Saxon density profiles and compared with ALICE results corresponding to (50–60)% and (60–70)% centralities of Pb-Pb collisions at $\sqrt{s_{NN}} = 5.02$ TeV. It can be clearly seen from the bottom panel of Fig. 6 that the results for OO collisions at $\sqrt{s_{NN}} = 7$ TeV for (0–5)% centrality agree well with the results for Pb-Pb collisions at $\sqrt{s_{NN}} = 5.02$ TeV for (50–60)% centrality, within uncertainties, and for both the density profiles. Hence, in this work, we have chosen to make a comparative study between the most central O-O collisions (0–5)% and the (50–60)% centrality class of Pb-Pb collisions.

B. R_{AA} vs. p_T

Prior to the estimation of R_{AA} for the oxygen system, we further investigated the goodness of the AMPT model in the calculation of this observable in Pb-Pb collisions. This investigation using the model and comparison of ALICE results for all charged hadrons are depicted in Fig. 7. These figures depict the p_T dependence of R_{AA} for both charged hadrons and

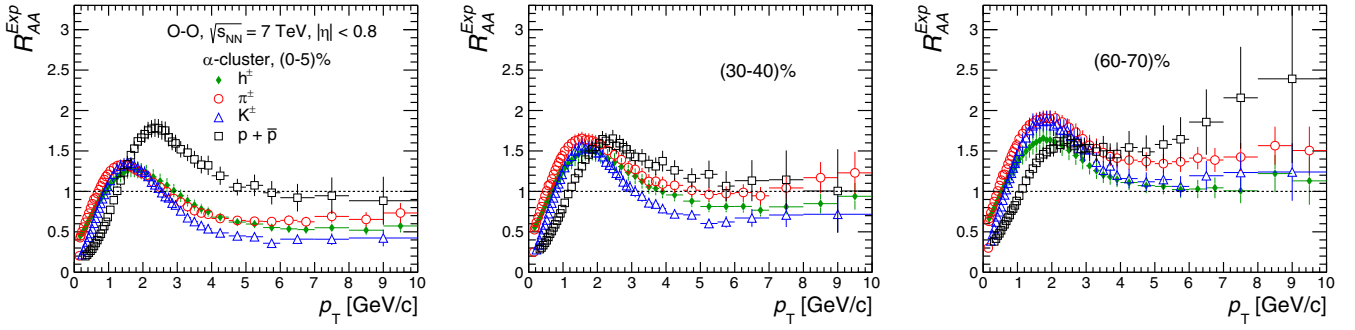


FIG. 8. Nuclear modification factor (R_{AA}) of all charged hadrons (h^\pm) and identified particles (π^\pm , K^\pm , and $p + \bar{p}$) in O-O collisions at $\sqrt{s_{NN}} = 7$ TeV for (0–5)% (left), (30–40)% (middle), and (60–70)% (right), with α -clustered nuclear structure, taking p_T spectra of pp from ALICE for estimating R_{AA} .

identified particles in the (50–60)% centrality class of Pb-Pb collisions at $\sqrt{s_{NN}} = 5.02$ TeV. Figure 7, top (bottom) shows the estimation of R_{AA} using the results of pp collisions from ALICE (AMPT) data. For both figures, the Pb-Pb yields are from the AMPT simulation. The comparison shows a substantial difference between simulation and experimental data towards $p_T < 4$ GeV. This discrepancy could be the consequence of the deviation observed in particle p_T spectra towards low- p_T range as seen in Fig. 1. Further, at $p_T > 3$ GeV, protons are observed to be less suppressed than other hadrons. The difference in species-specific suppression is compatible with a mass ordering towards $p_T < 1.5$ GeV, implicating radial flow [38]. At $p_T > 4$ GeV, a good agreement between experimental and AMPT models can be seen.

Now, we proceed to estimate R_{AA} in O-O collisions at $\sqrt{s_{NN}} = 7$ TeV. However, to study the effect of the nuclear density profile on the production of charged particles, we considered both α -clustered (Figs. 8 and 9) and Woods-Saxon (Figs. 10 and 11) density profiles. Also, to reflect on the effect of scaling of R_{AA} with p_T spectra obtained from pp collisions, Figs. 8 and 9 show results obtained considering scaling by ALICE experimental (AMPT simulated) data. The results are shown for the most central (0–5)%, mid-central (30–40)%, and peripheral (60–70)% collisions. From these Figs. 8–11, it is interesting to observe that a mass ordering between π^\pm , K^\pm , and protons remains conserved toward $p_T < 2$ GeV, de-

spite changes in density profiles and/or centralities. However, above $p_T > 2$ GeV, this pattern appears to break down for both density profiles. One can observe that R_{AA} values estimated using p_T spectra of pp collisions from AMPT (Figs. 9, 11) show a higher value than that obtained considering ALICE (Fig. 8, 10). It is worth mentioning here that in line with the findings of Ref. [39], where mesons such as $\phi(1020)$ and $K^{*0}(892)$ exhibit smaller R_{AA} values compared to protons at high p_T , we observe a similar trend among the identified particles clearly for the most central collisions. This trend suggests a baryon-meson ordering. The consequences of density profiles for O-O collisions are further explored in Fig. 12. Here, the ratio of R_{AA} of all charged hadrons considering α -clustered and Woods-Saxon density profiles are studied with transverse momentum at different centralities. It can be seen that at the most central collisions [(0–5)%], the effects of α -clustered and Woods-Saxon density profiles on charged hadrons yield are approximately the same. However, when transitioning from mid-central [(30–40)%] to peripheral [(60–70)%] collisions, considering the uncertainties, it becomes apparent that nuclei with oxygen and α -clustered density profiles have a more significant impact on particle production compared to those with Woods-Saxon density profiles. This suggests that colliding nuclei with α -clustered structure creates a compact and denser fireball, particularly in relatively noncentral collisions in comparison with the Woods-Saxon

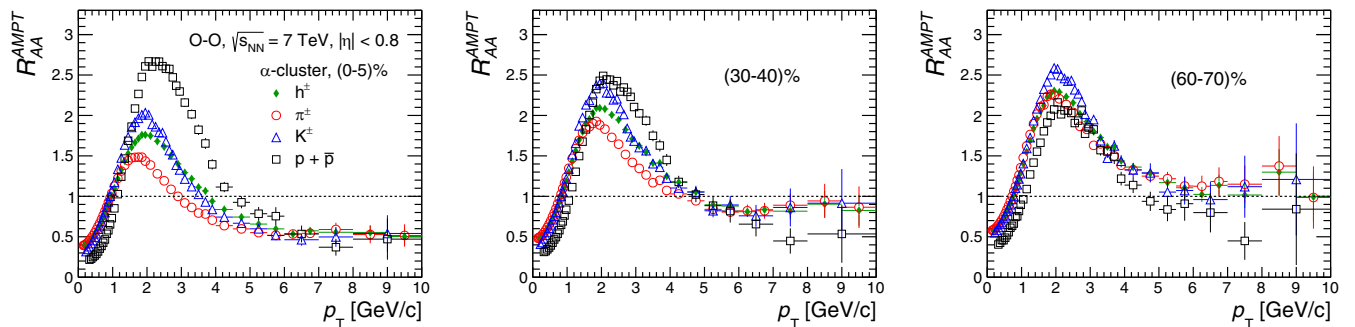


FIG. 9. Nuclear modification factor (R_{AA}) of all charged hadrons (h^\pm) and identified particles (π^\pm , K^\pm , and $p + \bar{p}$) in O-O collisions at $\sqrt{s_{NN}} = 7$ TeV for (0–5)% (left), (30–40)% (middle), and (60–70)% (right), with α -clustered nuclear structure, taking p_T spectra of pp from AMPT for estimating R_{AA} .

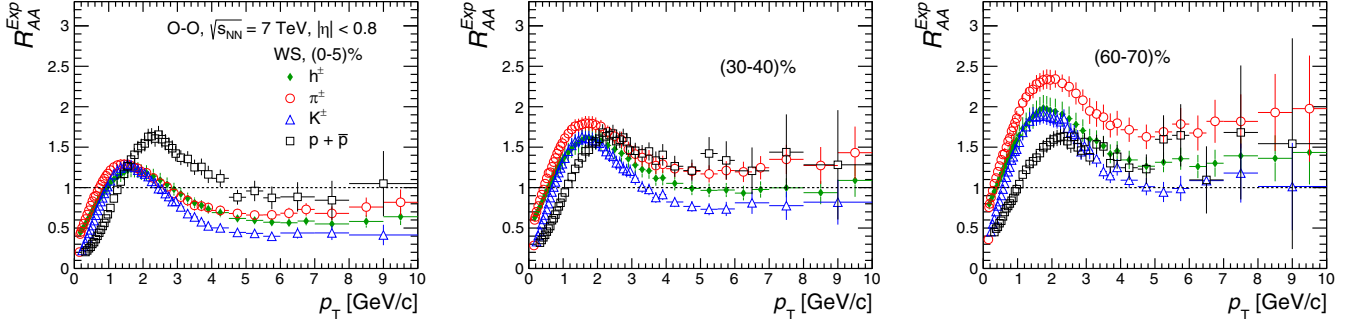


FIG. 10. Nuclear modification factor (R_{AA}) of all charged hadrons (h^\pm) and identified particles (π^\pm , K^\pm , and $p + \bar{p}$) in O-O collisions at $\sqrt{s_{NN}} = 7$ TeV for (0–5)% (left), (30–40)% (middle) and (60–70)% (right), with Woods-Saxon density profile, taking p_T spectra of pp from ALICE for estimating R_{AA} .

density profile. This finding sheds light on the intricate relationship between the nuclei’s internal structure, collision dynamics, and the subsequent particle production processes, contributing to a deeper understanding of the complex physics at play in O-O collisions.

On further examination of Figs. 8, 9 and Figs. 10, 11, it is observed that in the intermediate- p_T range ($1.5 \text{ GeV} < p_T < 3.0 \text{ GeV}$), R_{AA} reaches its maximum before declining towards high- p_T . This decline could be attributed to a single energy loss mechanism [21,40] that affects all particle species at high- p_T . In the low- and mid- p_T regions, radial boosts and p_T broadening help to explain the observed trends [41]. Radial boosts cause particles with low- p_T to move towards higher- p_T regions, resulting in reduced R_{AA} in the low- p_T region [40]. On the other hand, p_T broadening caused by multiple parton interactions leads to a noticeable peak in the p_T spectrum. Additionally, we observe that suppression is more pronounced in most central collisions compared to peripheral collisions. This could be attributed to the central collisions having relatively larger energy densities.

It was discussed in Sec. III that the (0–5)% centrality class of O-O collisions and the (50–60)% class of Pb-Pb collisions exhibit approximately similar multiplicities. To examine the consequences of this fact on the nuclear modification factor, we investigated the ratio of Pb-Pb (50–60)% collisions to

O-O (0–5)% collisions for all charged hadrons, considering both α -clustered and Woods-Saxon density profiles for oxygen nuclei. This ratio is shown in Fig. 13, demonstrates that the R_{AA} value in Pb-Pb collisions is smaller than in O-O collisions. Thus, the suppression effect is more pronounced in Pb-Pb collisions compared to O-O collisions within a similar multiplicity range. As observed in Ref. [8], Pb-Pb collisions exhibit a 60% larger radius than O-O collisions at a similar multiplicity. This observation implies that the partons traveling through the dense medium created in the Pb-Pb collisions (relatively larger nuclei) need to cover a longer path. As a result, this longer path length leads to increased energy loss when compared to O-O collisions. This observation is consistent with a study presented in Ref. [42], where the R_{AA} for Pb-Pb collisions and Xe-Xe collisions at similar multiplicity was examined.

C. R_{AA} variation with η

As we know, the particle production at midrapidity is primarily because of the gluon-rich medium. While at forward rapidity, the particle production mechanism is dominated by the constituent quarks. Therefore, it is of interest to study the rapidity dependence on the relative yield of the particles produced in ultrarelativistic collisions. Here in Fig. 14, we

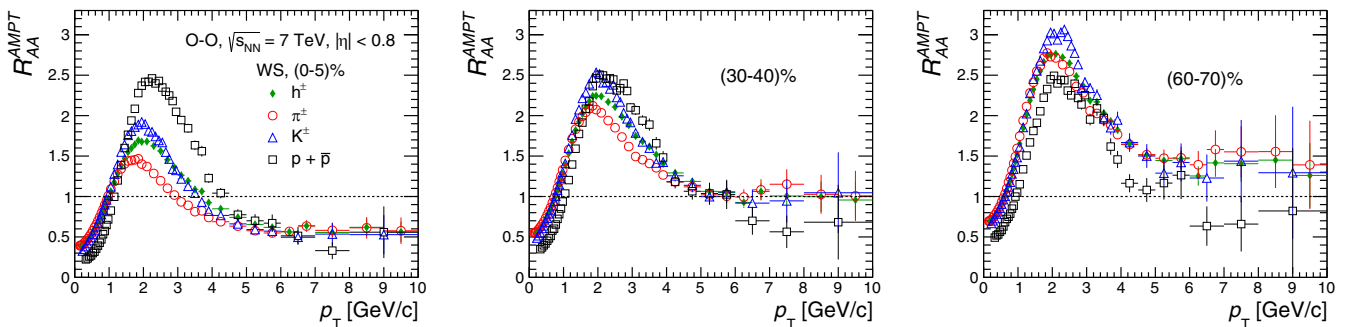


FIG. 11. Nuclear modification factor (R_{AA}) of all charged hadrons (h^\pm) and identified particles (π^\pm , K^\pm , and $p + \bar{p}$) in O-O collisions at $\sqrt{s_{NN}} = 7$ TeV for (0–5)% (left), (30–40)% (middle), and (60–70)% (right), with Woods-Saxon density profile, taking p_T spectra of pp from AMPT for estimating R_{AA} .

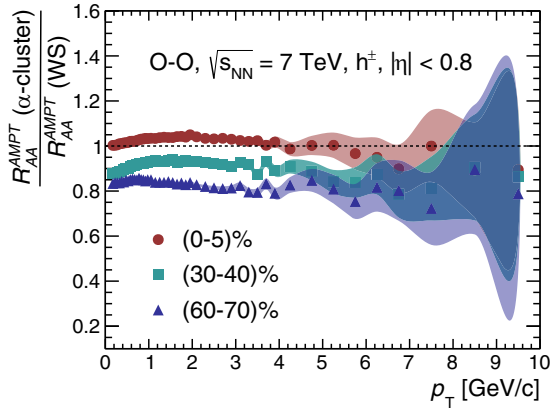


FIG. 12. Ratio between R_{AA} of α -clustered to Woods-Saxon density potential of all charged hadrons (h^\pm) in O-O collisions at $\sqrt{s_{NN}} = 7$ TeV. The shaded region shows the statistical errors.

depicted the R_{AA} for all charged hadrons in (0–5)% centrality class at midrapidity ($|\eta| < 0.8$) and forward-rapidity ($2 < \eta < 5$) interval for both α -cluster and Woods-Saxon density profiles in O-O collisions at $\sqrt{s_{NN}} = 7$ TeV. It is to be noted that the chosen rapidity regions have been taken from the Ref. [13]. The closed and open markers symbolize the nuclear modification factor obtained at midrapidity and forward rapidity, respectively. Figure 14 characterizes that the AMPT model predicts relatively less yield for all charged particles at forward rapidity compared with midrapidity up to $p_T \approx 3$ GeV. However, at $p_T > 3$ GeV, all the charged particles are suppressed with the same amount at midrapidity and forward rapidity. It implies that particles moving at high speed are independent of the phase space distribution. It is consistent with the phenomena, which suggest that the first moving particles escape the system before suffering any medium energy loss. We have also observed that the nuclear modification factor at a given rapidity is independent of Woods-Saxon and α -cluster density profiles.

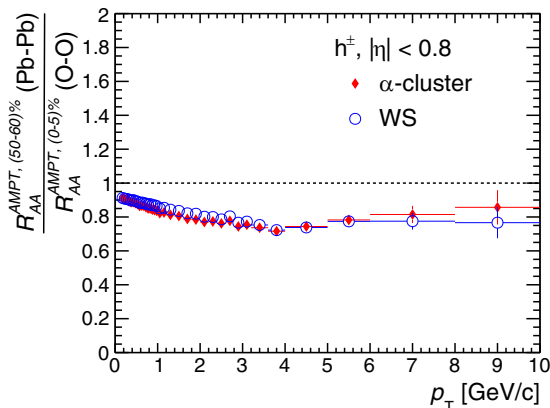


FIG. 13. Ratio between R_{AA} in Pb-Pb collisions of (50–60)% at $\sqrt{s_{NN}} = 5.02$ TeV to O-O collisions of (0–5)% at $\sqrt{s_{NN}} = 7$ TeV for charged hadrons. Statistical errors are within the markers.

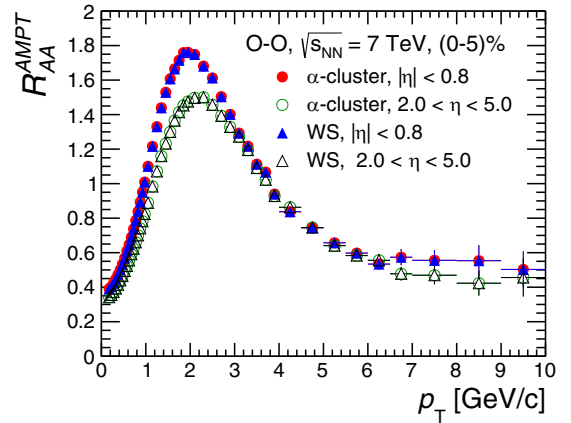


FIG. 14. Rapidity dependency of nuclear modification factor of charged hadrons in O-O collisions at $\sqrt{s_{NN}} = 7$ TeV for (0–5)% centrality class.

IV. SUMMARY

This study investigates the nuclear modification factor (R_{AA}) for upcoming O-O collisions at $\sqrt{s_{NN}} = 7$ TeV at the LHC using a transport model. We consider the centrality of O-O collisions to be in a QCD environment similar to that of Pb-Pb collisions at $\sqrt{s_{NN}} = 5.02$ TeV, with respect to the final-state charged-particle multiplicity. Additionally, we explore the dependence on density profiles, including Woods-Saxon and α -clustered profiles. Finally, we study the rapidity dependence of the nuclear modification factor for O-O collisions at $\sqrt{s_{NN}} = 7$ TeV. The key findings, with regard to the O-O collisions are summarized below:

- (i) It is observed that the nuclear modification factor (R_{AA}) of charged hadrons and identified particles for O-O collisions have a smaller value for the most central (0–5)% collisions in comparison to the peripheral collisions (60–70)%, regardless of the density profiles used.
- (ii) It is observed that the mass ordering among the identified particles remains consistent in the low- p_T region (< 2 GeV), irrespective of changes in density profiles and/or centralities. However, this trend ceases to exist for $p_T > 2$ GeV. In this context, a baryon-meson ordering becomes evident towards high- p_T and is particularly prominent in most central collisions.
- (iii) We have observed that the R_{AA} values obtained using the p_T spectra of pp collisions from the AMPT simulation exhibit higher values compared to those obtained using ALICE data. This shows that the production of hadrons is more in pp collisions at ALICE than in the AMPT simulation, highlighting the inadequacy of the AMPT model.
- (iv) From the study of R_{AA} for charged hadrons and identified particles, we additionally observe that the effect of α -clustered density profiles on particle production is more pronounced in mid-central and peripheral collisions compared to the most central collisions,

as opposed to the Woods-Saxon density profile. This suggests that the nuclei with α -clustered structure colliding may generate a more compact and denser fireball, particularly in relatively noncentral collisions.

- (v) Furthermore, we observe that despite having the same final-state multiplicity, the (50–60)% centrality class of Pb-Pb collisions displays greater suppression than the (0–5)% centrality class of O-O collisions. This underscores the significance of the system size to which the hadrons are exposed. Thus, here, Pb-Pb collisions create a larger nuclear environment compared to O-O collisions.
- (vi) In the context of rapidity dependence, we observed a relatively lower yield at forward rapidity compared to midrapidity for charged hadrons in O-O collisions at

$\sqrt{s_{\text{NN}}} = 7$ TeV. The nuclear modification factor in a given rapidity window is found to be independent of nuclear density profiles.

ACKNOWLEDGMENTS

D.B. acknowledges the support of a doctoral fellowship from CSIR, the Government of India. S.D. acknowledges the financial support from the postdoctoral fellowship of CNRS at IJCLAB, Orsay, France. R.S. and C.R.S. acknowledge the financial support under the ALICE project (Project No. SR/MF/PS-02/2021-IITI (E-37123)). The usage of the ALICE Tier-3 computing facility at IIT Indore is gratefully acknowledged. The authors would like to acknowledge the help from Neelkamal Mallick related to the MC implementation of α -clustering density profile in the oxygen nucleus.

-
- [1] J. Adam *et al.* (ALICE Collaboration), *Nature Phys.* **13**, 535 (2017).
 - [2] V. Khachatryan Jr. *et al.* (CMS Collaboration), *Phys. Lett. B* **765**, 193 (2017).
 - [3] J. Brewer, A. Mazeliauskas, and W. van der Schee, [arXiv:2103.01939](https://arxiv.org/abs/2103.01939).
 - [4] S. Acharya *et al.* (ALICE Collaboration), ALICE-PUBLIC-2021-004 (2021), <https://cds.cern.ch/record/2765973?ln=en>.
 - [5] S. H. Lim, J. Carlson, C. Loizides, D. Lonardon, J. E. Lynn, J. L. Nagle, J. D. Orjuela Koop, and J. Ouellette, *Phys. Rev. C* **99**, 044904 (2019).
 - [6] M. Rybczyński and W. Broniowski, *Phys. Rev. C* **100**, 064912 (2019).
 - [7] S. Huang, Z. Chen, J. Jia, and W. Li, *Phys. Rev. C* **101**, 021901(R) (2020).
 - [8] M. D. Sievert and J. Noronha-Hostler, *Phys. Rev. C* **100**, 024904 (2019).
 - [9] B. Schenke, C. Shen, and P. Tribedy, *Phys. Rev. C* **102**, 044905 (2020).
 - [10] B. G. Zakharov, *J. High Energy Phys.* **09** (2021) 087.
 - [11] A. Huss, A. Kurkela, A. Mazeliauskas, R. Paatelainen, W. van der Schee, and U. A. Wiedemann, *Phys. Rev. C* **103**, 054903 (2021).
 - [12] G. Röpke, P. Schuck, C. Xu, Z. Ren, M. Lyu, B. Zhou, Y. Funaki, H. Horiuchi, A. Tohsaki, and T. Yamada, *J. Low Temp. Phys.* **189**, 383 (2017).
 - [13] D. Behera, N. Mallick, S. Tripathy, S. Prasad, A. N. Mishra, and R. Sahoo, *Eur. Phys. J. A* **58**, 175 (2022).
 - [14] Y. A. Li, S. Zhang, and Y. G. Ma, *Phys. Rev. C* **102**, 054907 (2020).
 - [15] Z. W. Lin, C. M. Ko, B. A. Li, B. Zhang, and S. Pal, *Phys. Rev. C* **72**, 064901 (2005).
 - [16] C. Zhang, L. Zheng, F. Liu, S. Shi, and Z. W. Lin, *Phys. Rev. C* **99**, 064906 (2019).
 - [17] X. N. Wang and M. Gyulassy, *Phys. Rev. D* **44**, 3501 (1991).
 - [18] B. Zhang, *Comput. Phys. Commun.* **109**, 193 (1998).
 - [19] Z. W. Lin and L. Zheng, *Nucl. Sci. Tech.* **32**, 113 (2021).
 - [20] B. B. Abelev *et al.* (ALICE Collaboration), *Eur. Phys. J. C* **73**, 2662 (2013).
 - [21] S. Acharya *et al.* (ALICE Collaboration), *J. High Energy Phys.* **11** (2018) 013.
 - [22] J. Adam *et al.* (ALICE Collaboration), *Phys. Lett. B* **760**, 720 (2016).
 - [23] J. Adam *et al.* (ALICE Collaboration), *Eur. Phys. J. C* **75**, 226 (2015).
 - [24] C. Ding, L. G. Pang, S. Zhang, and Y. G. Ma, *Chin. Phys. C* **47**, 024105 (2023).
 - [25] Y. Z. Wang, S. Zhang, and Y. G. Ma, *Phys. Lett. B* **831**, 137198 (2022).
 - [26] M. Rybczyński, M. Piotrowska, and W. Broniowski, *Phys. Rev. C* **97**, 034912 (2018).
 - [27] A. Svetlichnyi, S. Savenkov, R. Nepeivoda, and I. Pshenichnov, *Physics* **5**, 381 (2023).
 - [28] D. Behera, S. Prasad, N. Mallick, and R. Sahoo, *Phys. Rev. D* **108**, 054022 (2023).
 - [29] J. Adam *et al.* (ALICE Collaboration), *Phys. Rev. Lett.* **116**, 222302 (2016).
 - [30] L. D. Landau, *Izv. Akad. Nauk. SSSR* **17**, 51 (1953); S. Z. Belen’kii and L. D. Landau, *Usp. Fiz. Nauk.* **56**, 309 (1955); S. Z. Belen’kii, *Nuovo Cimento Suppl.* **3**, 15 (1956); D. ter Haar, *Collected Papers of L. D. Landau* (Gordon & Breach, New York, 1965), pp. 665–700.
 - [31] L. Van Hove, *Phys. Lett. B* **118**, 138 (1982).
 - [32] B. B. Abelev *et al.* (ALICE Collaboration), *Phys. Lett. B* **727**, 371 (2013).
 - [33] M. L. Miller, K. Reygers, S. J. Sanders, and P. Steinberg, *Annu. Rev. Nucl. Part. Sci.* **57**, 205 (2007).
 - [34] C. Loizides, *Phys. Rev. C* **94**, 024914 (2016).
 - [35] R. J. Glauber and G. Matthiae, *Nucl. Phys. B* **21**, 135 (1970).
 - [36] A. Huss, A. Kurkela, A. Mazeliauskas, R. Paatelainen, W. van der Schee, and U. A. Wiedemann, *Phys. Rev. Lett.* **126**, 192301 (2021).
 - [37] C. Loizides, J. Kamin and D. d’Enterria, *Phys. Rev. C* **97**, 054910 (2018); **99**, 019901(E) (2019).
 - [38] S. Acharya *et al.* (ALICE Collaboration), *Phys. Rev. C* **101**, 044907 (2020).
 - [39] J. Adam *et al.* (ALICE Collaboration), *Phys. Rev. C* **95**, 064606 (2017).
 - [40] F. X. Liu, Z. L. She, H. G. Xu, D. M. Zhou, G. Chen, and B. H. Sa, *Sci. Rep.* **12**, 1772 (2022).
 - [41] J. W. Cronin *et al.* (E100 Collaboration), *Phys. Rev. D* **11**, 3105 (1975).
 - [42] S. Acharya *et al.* (ALICE Collaboration), *Phys. Lett. B* **788**, 166 (2019).